ATMOSPHERIC RESEARCH

RECHERCHE ATMOSPHÉRIQUE

ATMOSPHERIC ENVIRONMENT

ENVIRONNEMENT ATMOSPHÉRIQUE

Report - ARQL - 2/77

Digital Simulation of Turbulence in the Atmospheric Boundary Layer
I - Linear Representation

by

Bryan R. Kerman

Boundary Layer Research Division,
Air Quality and Inter-Environmental Research Branch,
Atmospheric Environment Service,
Downsview, Ontario.

1. The Problem

As man-made structures have been made larger and more flexible, it has become imperative that the effects of the wind, both as a static and fluctuating force, be incorporated in structural and economic designs. In addition, in response to increasing concern for the quality of the environment, the need to understand the wind-driven diffusion mechanism distributing air-borne pollutants through the atmospheric environment has increased. An important difficulty lies in incorporating the wealth of information about the statistical structure of the wind, particularly near the ground into applications in a manner that is at once practical and realistic as it conveys important aspects of the meteorological dynamics of the problem.

Of course, not all requirements for simulating the statistical structure of the wind field can be met by developing a particular model. For example, the methods used to simulate the dynamics of turbulence (Kraichnam, 1965; Herring, 1966; Deardorff, 1972a), while useful in testing the consequences of the approximations characterizing each model, are either not theoretically compatible with the inhomogeneous structure of turbulence in the atmospheric boundary layer or else are impractical to implement.

The method found most suitable by engineers for simulating turbulence is the so-called spectral filtering, or forcing, technique pioneered by Liepmann (1954). The spectral filtering model essentially characterizes the response of an aircraft or structure, or any process driven by turbulence, as a signal derived by filtering a sequence of pulses uncorrelated sequentially whose amplitudes are derived probabilistically from a Gaussian distribution. The desirable property of the latter process is the constant spectrum, which, from optics, is referred to as a white spectrum. Because of the wide variety of applications (Houbolt, 1973), the method remains a useful technique. Its success to a considerable degree is attributable to its simplicity.

The linear spectral representation of turbulence has provided a useful interface between the meteorologist and the engineer. Consequently, its properties, successes and failures are well known to both. The interest of the meteorologist has been generally centered on providing the best possible estimates about the structure of the wind field, both as they relate to the vertical distribution of the averaged wind and to the spectral distribution of the fluctuating wind.

Models to simulate turbulence which require the specification of the mean wind with height and thermal stratification vary in their sophistication and reliance on the principles of boundary layer similarity. As a result, the description of the vertical profile of wind has tended to be a potpourri of empirical relationships and approximations. Because the numerous parameters which characterize turbulence in the atmospheric boundary layer have often not been measured simultaneously, the applicability of some empirical results is unknown.

Accordingly, there is a need to consolidate aspects of the vertical structure of the wind, in order to have them consistent with known similarity properties of the flow, and to be able to incorporate further results as they become available.

Another crucial feature of simulation models of turbulence near the ground is the approximation used for the spectral distribution of the variance in the fluctuating components of the wind, particularly, in the range of scales of size equal to or less than the distance, z, from the ground. Simulation models which lead to modeled realizations of the turbulence have required the so-called Dryden spectral form, which for sufficiently small scales varies as k^{-2}, where k is the wave number. This spectral form has no basis in theory or observations and has been chosen primarily for its analytical properties. Other applications not requiring modeled realizations have been based on the von Kármán spectral form which tends to $k^{-5/3}$, for $kz \gg 1$, in accordance with the well-known properties of the Kolmogorov inertial subrange. However, the von Kármán spectrum requires the specification of a length with which to characterize the bandwidth of the spectrum, but this length parameter bears no known dynamical relationship to the structural properties of the turbulence in the atmospheric boundary layer. It remains to determine alternative spectral forms which are

dynamically consistent with, say, the vertical profile of wind and dissipation determined by similarity arguments.

It is also well known that the concept of a linear representation of turbulence in terms of a Gaussian, white noise process is inconsistent with the observed non-Gaussian and non-linear structure of the turbulence. In particular, linear Gaussian models are inadequate for the simulation of the large gust structure. An extension of the representation of turbulence is considered a companion paper (Kerman, 1977) which systematically incorporates some basic properties of the non-linear and non-Gaussian probabilistic structure of the turbulence. The mathematical formulation of this extension is most conveniently based on a functional series expansion in terms of the simple and convenient Gaussian, white noise process -- the same as is used in linear modeling.

The method of functional representation will be shown to lead naturally to a concept of a discrete gust form. As such, the method of the representation is superior to other discrete gust models where mathematically convenient, ad hoc forms are specified. Because the discrete gust form is here a derived property of the process, a consistent formulation for the statistical structure of the turbulence in the boundary layer allows for a systematic analysis of this discrete gust form for various meteorological effects.

In summary, it is the purpose of this study to consolidate the simulation modeling of turbulence in the boundary layer in terms of boundary layer similarity principles and empirical results. It is also the intention of this work to identify some properties of the discrete gust form structure of the modeled turbulence.

2. Structure of the Atmospheric Boundary Layer

For a steady, horizontally homogeneous mean flow in the boundary layer, sufficiently near the ground, the vertical variation of the turbulence fluxes is negligible (Blackadar and Tennekes, 1968); in particular

$$\tau(z)/\rho_o = -\overline{uw} = u_*^2 \tag{1}$$

and

$$H(z)/\rho_o c_p = \overline{w\theta} = -u_* T_* \tag{2}$$

are independent of height. In (1) and (2), τ/ρ_o and $H(z)/\rho_o c_p$ are the specific momentum and heat fluxes respectively; ρ_o is the density of the air and c_p the specific heat at constant pressure. Equations (1) and (2) also serve as definitions for the characteristic velocity, u_*, and temperature T_*. According to the hypothesis of Monin and Oboukhov (1954) the structure of the mean wind shear and temperature gradient (sufficiently near the ground so that inertial effects due to the earth's rotation are unimportant) can be derived on the basis of dimensional arguments. That is, the mean shear and temperature gradient are given by

$$\frac{\partial \overline{U}}{\partial z} = \frac{u_*}{\kappa z}\,\phi_m(z/L) \tag{3}$$

and

$$\frac{\partial \overline{\theta}}{\partial z} = \frac{T_*}{\kappa z}\,\phi_h(z/L) \tag{4}$$

where L, the Monin-Oboukhov length, is

$$L = -\frac{u_*^2 T_o}{g\,\kappa\,T_*} \tag{5}$$

In (3) to (5), $\bar{U}$ is the mean wind speed, $\bar{\theta}$ the mean potential temperature, T_o the depth averaged boundary temperature, κ (a similarity parameter) is von Kármán's constant, and ϕ_m and ϕ_h are the similarity functions for the shear and the temperature gradient. It is convenient in what follows to define z/L by

$$\zeta = z/L \tag{6}$$

In fact, the Monin-Oboukhov hypothesis states that all statistics of the turbulence sufficiently near the ground, in thermally stratified steady, horizontally homogeneous flows, become functions of ζ only, if velocities are scaled with u_*, temperatures by T_* and lengths by κz. Accordingly the moments M_i^n, of the probabilistic density function of the i^{th} turbulence velocity components are also functions of ζ,

$$\overline{u_i^n} = M_i^n(\zeta) \tag{7}$$

The spectral distribution, Φ_{ij}, of variance or covariance over the range of wave numbers, κ, for which there is any shear or buoyantly induced turbulence, becomes, under the appropriate scaling,

$$\frac{k\,\Phi_{ij}}{S_i S_j} = G_{ij}(f,\zeta) \tag{8}$$

In (8), S_i represents the appropriate scaling variable, u_* or T_*, and f, where

$$f = \kappa z\, k \quad , \tag{9}$$

represents a normalized wave number. The use of subscripts 1 through 3 assumes the standard meteorological usage (Lumley and Panofsky, 1964) and a subscript θ refers to temperature.

For scales, f >> 1, such that the turbulence becomes asymptotically independent of the details of the mechanisms generating the turbulence (Tennekes and Lumley, 1972, Chapter 8), the spectra, G_{ii} are similar, in the sense of dimensional analysis, under the hypotheses of Kolmogorov (1941), so that

$$G_{ii}(f) = \alpha_i \, \phi_{ii}(\zeta) \, f^{-2/3} \tag{10}$$

Specifically, for a sufficiently large Reynolds number, defined by

$$R_\ell = \kappa z \, u_* / \nu \tag{11}$$

where ν is the kinematic viscosity,

$$\phi_{11} = \phi_{22} = \phi_{33} = \phi_\varepsilon^{2/3}(\zeta) \tag{12}$$

and

$$\phi_{\theta\theta} = \phi_\chi(\zeta) \, \phi_\varepsilon^{-1/3}(\zeta) \tag{13}$$

The functions ϕ_χ and ϕ_ε represent the similarity functions under Monin-Oboukhov scaling, for the dissipation rates of kinetic energy, ε, and temperature variance, χ, and are defined by

$$\phi_\varepsilon(\zeta) = \kappa z \varepsilon / u_*^3 \tag{14}$$

and

$$\phi_\chi(\zeta) = \kappa z \chi / u_* T_*^2 \quad . \tag{15}$$

A considerable effort has been made by many investigators to identify the similarity structure, both of the low order moments of turbulence near the ground, under thermally stratified conditions, and of the spectral and co-spectral forms. An excellent summary and review is provided by several authors in a monograph edited by Haugen (1973), and will not be duplicated here. A summary of empirical forms for ϕ_m, ϕ_h, ϕ_ε, ϕ_χ, and M_i^n, as functions of ζ, are given in Kerman (1975, Appendix A), as well as empirical spectra and co-spectra, G_{ij}, as functions of ζ and f.

In order to utilize the similarity relationships of Monin and Oboukhov, it is necessary to estimate the factors u_* and T_* by an independent method. For a steady, horizontally homogeneous boundary layer, Kazanski and Monin (1961) derived the so-called resistance laws

$$\ln(G/fz_o) = B + \ln (G/u_*) + (\kappa^2 G^2/u_*^2 - A^2)^{1/2} \tag{16}$$

and

$$\sin \alpha = - \frac{A}{\kappa} \frac{u_*}{G} \tag{17}$$

In (16) and (17), G is the geostrophic wind modulus and f is the Coriolis parameter (= $2\Omega \sin \psi$ where Ω is the earth's angular velocity and ψ is latitude), α is the angle between the direction of the surface stress and the geostrophic velocity, and z_o is the surface roughness. The functions, A and B, are similarity functions, which for diabatic conditions are hypothesized to be universal in the stability parameter, μ, given by

$$\mu = h/L \tag{18}$$

where h is the so-called Ekman height

$$h = \kappa u_*/f \tag{19}$$

characteristic of the depth of the boundary layer under neutral stratification. An analogous development by Zilitinkevich and Chalikov (1968) for the transfer of heat across a turbulent boundary layer is given by

$$\Delta\theta/T_* = P_o[\ln(u_*/f\, z_o) - C(\mu)] \tag{20}$$

where $\Delta\theta$ is defined as the potential temperature difference between the surface and the level where the flow is geostrophic, P_o is the turbulent Prandtl number ($\simeq 0.7$) under near-neutral conditions and C is a universal function of μ. From empirical formulations for $A(\mu)$, $B(\mu)$ and $C(\mu)$, Arya, 1972), it is possible to construct algorithms for the momentum drag coefficient, u_*/G and the 'thermal drag' coefficient, $T_*/\Delta\theta$, as functions of the dimensionless parameters, Ro and S_g, given by

$$Ro = G/fz_o \tag{21}$$

and

$$S_g = g/T_o(\Delta\theta/Gf) \tag{22}$$

Accordingly, u_* and T_* can be derived immediately given the external, controlling variables of the problem -- G, z_o, and $\Delta\theta$. Refinements to resistance law formulations to include the actual boundary layer depth are discussed by Zilintinkevich (1975).

It is emphasized here that since the basic meteorological dynamics, as conveyed by the similarity theories, are self-consistent with the empirical representations (such as given in Kerman, 1975), it is pointless to introduce additional variables through ad hoc models of the spectra. That is, in models such as von Kármáns's (Teunnissen, 1970, p. 40) the scaling lengths there are not linked dynamically to similarity theories. In fact, it is often observed that a form other than the von Kármán spectral form, may be appropriate for representing the large scale structure of the spectrum. For these reasons, only spectra based on direct observations are considered in the models developed here.

3. Formulation of the Simulation Model

In order to extend the methods of simulating turbulence to processes with rather general spectral and non-Gaussian characteristics, it is necessary to develop a suitable mathematical structure and explore some of its properties. We now outline a particular functional representation for turbulence that allows for a systematic development based on a Gaussian process.

a) A Functional Representation of Turbulence

Volterra (1930) showed that a continuous functional (transformation) could be uniquely approximated by a polynomial series of functionals given by

$$\begin{aligned} y(t) = K^{o} + \int_{-\infty}^{\infty} K^{1}(t;t_1)\, \xi(t_1)\, dt_1 + \int_{-\infty}^{\infty}\int_{-\infty}^{\infty} \\ K^{2}(t;t_1,t_2)\, \xi(t_1)\, \xi(t_2)\, dt_1\, dt_2 \\ + \int_{-\infty}^{\infty}\int_{-\infty}^{\infty}\int_{-\infty}^{\infty} K^{3}(t;t_1,t_2,t_3)\, \xi(t_1)\, \xi(t_2)\, \xi(t_3) \\ dt_1\, dt_2\, dt_3 + \ldots \end{aligned} \tag{23}$$

(All integrals hereafter will have a range $(-\infty, \infty)$ unless otherwise specified). The functions, K^{i}, are referred to as the kernals of the representation. A physically realizable situation, in which the transformation of any signal can act only on the past of an input, requires that

$$K^{i}(t;t_1,t_2,\ldots t_i) \qquad (t_i > t) \tag{24}$$

For a horizontally homogeneous turbulent flow whose statistics are advected according to Taylor's hypothesis, the turbulent process is also temporally invariant, or stationary, so that

$$K^{i}(t;t_1,t_2,\ldots t_i) = K^{i}(t-t_1, t-t_2, \ldots, t-t_i) \tag{25}$$

In addition to determining the transformation of the input to the output functions, the kernels also determine the statistics of the output from those of the input. A simple, linear, temporally invariant system is represented by

$$y(t) = \int K^1(t-\tau)\ \xi(\tau)\ d\tau \quad . \tag{26}$$

For convenience, we take the input to have zero mean ($\overline{\xi} = 0$).

Formation of statistical averages of the input and output leads to

$$\overline{y(t)\ y(t+\tau)} = R_{yy}(\tau) = \iint K^1(\tau_1)\ \overline{R_{\xi\xi}(\tau+\tau_1+\tau_2)}\ d\tau_1\ d\tau_2 \tag{27}$$

and

$$\overline{y(t)\ \xi(t+\tau)} = R_{t\xi}(\tau) = \int K^1(\tau_1)\ \overline{R_{\xi\xi}(\tau-\tau_1)}\ d\tau_1 \quad , \tag{28}$$

In (27), the output variance, R_{yy}, is represented as a transformation of the input variance, $R_{\xi\xi}$. The utility of using a white-noise input process, defined by

$$R_{\xi\xi}(\tau) = \delta(\tau) \tag{29}$$

(δ is the Dirac delta function) is shown by substituting (29) in (27) and (28) to form

$$R_{yy}(\tau) = \int K^1(\tau_1)\ K^1(\tau-\tau_1)\ d\tau_1 \tag{30}$$

$$R_{y\xi}(\tau) = K^1(\tau) \tag{31}$$

The kernel, K^1, is therefore derivable by cross-correlating the input and output, and the kernels for the functional transformation of the white noise process share variance properties with the output.

It is important to note that while the above technique of determining the kernel of a linear system is used in many fields of engineering, here the supposition that both the input pulse and output response are available for correlation is not valid. The input forcing mechanism, as represented by the functional transformation (23), is internal to the fluid and not measurable. This makes the problem of determining the kernels in practice more complicated than the usual situation where both input and output are available simultaneously.

The significance of (30) is better seen in a spectral representation. Consider a Fourier transform defined by

$$f(t) = \frac{1}{2\pi} \int \hat{f}(\omega) e^{-i\omega t} \, d\omega \tag{32}$$

applied to (26). The result is given by

$$\hat{y}(\omega) = \hat{K}^1(\omega) \, \hat{\xi}(\omega) \tag{33}$$

which for the white-noise property

$$|\hat{\xi}|^2 = 1 \tag{34}$$

becomes

$$|\hat{y}|^2 = |\hat{K}^1|^2 \tag{35}$$

Thus the spectrum of the kernel is equal to that of the output for a linear system. Equation 35 forms the basis for many of the applications of the linear simulation of turbulence. A major question remaining, then, is how to determine K^1, given that its spectrum is that of the turbulence. A recent computational development is explored later to determine K^1 for a relatively general class of spectra.

An important consideration in developing a simulation model is the ease of application. Parente (1970) has outlined the method of treating interacting systems. In most applications of turbulence models, the simulated turbulence is used in turn to stimulate a system representing a structure or perhaps another geophysical process. By the algebra of functionals (Parente), the final response statistics are derivable from those of the turbulence without recourse to actually generating simulated realizations. Of course, such a consideration is basic to linear filtering, but it is useful to note that its application is also valid with non-linear simulations such as discussed in the companion paper (Kerman, 1977).

As shown by Barrett (1963), the functional expansion of (23) can be made more efficient by an orthogonalization of the basis, or input process, $\xi(t)$. The question is what process to use for maximum efficiency. To this end, it is useful to consider the probabilistic structure of boundary layer turbulence.

b) Probabilistic Structure of Surface Turbulence

For many years (Batchelor, 1953) the one-point turbulent velocity probability density function (p.d.f.) was observed to be indistinguishable from a Gaussian distribution. Stewart (1951) was the first to establish the pronounced non-Gaussian structure of turbulence with decreasing scale. Further investigations of the moment distributions over scale (Frenkiel and Klebanoff, 1967) confirm the converse of Stewart's work -- that there is a quasi-Gaussian structure at scales commensurate with the energy containing sizes.

Arguments concerning Gaussian structure are not extendable to the joint p.d.f. of two velocities at neighboring points because of the non-linear effects (Batchelor, Chapter VIII) which lead to an inertial transfer of energy across wave-numbers. Because non-linear interactions within the turbulence increase with decreasing scale up to the viscous limit, a resulting increase of non-Gaussian characteristics with decreasing scale is to be expected. The probability distribution of the dissipation rate

$$\epsilon = 15\nu \left(\overline{\frac{\partial u}{\partial x}}\right)^2 \tag{36}$$

for isotropic turbulence (or equivalently local accelerations) is a convenient measure of the non-linear (and non-Gaussian) structure over a wide wavenumber region of engineering concern. According to Kolmogorov (1962), Oboukhov (1962) and Grant et al. (1962), the equilibrium structure implied in Kolmogorov's original similarity result required a refinement to a more local, volume-averaged dissipation rate, $< \varepsilon >$. It has been suggested (Gurvich and Yaglom, 1967) that $< \varepsilon >$ has a log-normal distribution. This prediction has been disputed by Tennekes and Wyngaard (1972) and Gibson and Masiello (1971) on the basis of experimental data taken at a very large Reynolds number. At present, the only workable hypotheses on the probability structure appear to be empirical (Tennekes and Wyngaard, 1972; Frenkiel and Kelbanoff, 1967).

Therefore, it is reasonable to attempt a simulation of the energy containing structure of surface layer turbulence in terms of a quasi-Gaussian process. The fact that the observed structure of the surface layer turbulent velocity field is nearly Gaussian (Kerman, 1975, Appendix A), as expected by the preceding discussion, is encouraging for modeling purposes.

c) Wiener-Hermite Functional Representation

The orthogonal functional polynomials based on input realizations, $\xi(t)$, drawn from a white, Gaussian, stationary process are (Barrett, 1963) the Hermite polynomials given by

$$H_o(\xi) = 1 \tag{37}$$

$$H_1(t_1;\xi) = \xi(t_1) \tag{38}$$

$$H_2(t_1,t_2;\xi) = \xi(t_1)\,\xi(t_2) - \delta(t_1-t_2) \tag{39}$$

$$H_3(t_1,t_2,t_3;\xi) = \xi(t_1)\,\xi(t_2)\,\xi(t_3) - \xi(t_1)\,\delta(t_2-t_3) - \xi(t_2)\,\delta(t_3-t_1) - \xi(t_3)\,\delta(t_1-t_2) \tag{40}$$

The Wiener-Hermite (hereafter referred to W-H) representation of a velocity component, $u(t)$, by a white, Gaussian, stationary process is given by

$$\begin{aligned} u(t) = & \int K^1(t-t_1)\, H_1(t_1)\, dt_1 \\ & + \iint K^2(t-t_1, t-t_2)\, H_2(t_1, t_2)\, dt_1\, dt_2 \\ & + \iiint K^3(t-t_1, t-t_2, t-t_3)\, H_3(t_1, t_2, t_2)\, dt_1\, dt_2\, dt_3 + \ldots \end{aligned} \tag{41}$$

where both input, $\xi(t)$, and output, $u(t)$, are understood to have a mean of zero. An equivalent representation follows from a Fourier transformation (32) of (41)

$$\begin{aligned} \hat{u}(\omega) = & \hat{K}^1(\omega)\, \hat{H}_1(\omega) + \int \hat{K}^2(\omega_1, \omega-\omega_1)\, \hat{H}_2(\omega_1, \omega-\omega_1)\, d\omega_1 \\ & + \ldots \end{aligned} \tag{42}$$

The orthogonality conditions for the Hermite-polynomials given by

$$\overline{H_o(t_1;\xi)\, H_o(t_2;\xi)} = 1 \tag{43}$$

$$\overline{H_1(t_1;\xi)\, H_2(t_2;\xi)} = \delta(t_1 - t_2) \tag{44}$$

$$\begin{aligned} \overline{H_2(t_1, t_2;\xi)\, H_2(t_3, t_4;\xi)} = & \delta(t_1 - t_3)\, \delta(t_2 - t_4) \\ & + \delta(t_1 - t_4)\, \delta(t_2 - t_3) \end{aligned} \tag{45}$$

or, their Fourier transformed equivalent,

$$\overline{\hat{H}_1(\omega_1)\, \hat{H}_1(\omega_2)} = \delta(\omega_1 + \omega_2) \tag{46}$$

$$\begin{aligned} \overline{\hat{H}_2(\omega_1, \omega_2)\, \hat{H}_2(\omega_3, \omega_4)} = & \delta(\omega_1 + \omega_3)\, \delta(\omega_2 + \omega_4) \\ & + \delta(\omega_1 + \omega_4)\, \delta(\omega_2 + \omega_3) \end{aligned} \tag{47}$$

considerably reduce the complexity of computing the output statistics. For example, by utilizing the orthogonality conditions, the expression for the spectral density of the u-process, ϕ_u, defined by

$$\overline{\hat{u}(\omega_1)\,\hat{u}(\omega_2)} = \phi_u(\omega_1)\,\delta(\omega_1+\omega_2) \tag{48}$$

is given by

$$\phi_u(\omega) = |\hat{K}^1(\omega)|^2 + \frac{1}{\pi}\int |K^2(\omega_1,\omega-\omega_1)|^2\, d\omega_1 + \ldots \tag{49}$$

Equation (49) expresses the decomposition of the spectrum of the process into a sequence of positive definite contributions. The positive definiteness of the W-H representation is a desirable feature of the method. Not every moment expansion scheme (Ogura, 1963; Deardorff, 1972b) can guarantee such a property, and in this respect these other methods contain basic inconsistencies. The implicit assumption made in using the W-H representation as a representation of nearly Gaussian process is that the contributions to the spectrum will tend to concentrate the variance in the low order terms of (49). Because the Hermite polynomials, and hence individual Hermite functionals of the expansion (41) and (42) are orthogonal, the truncation

$$K^i = 0 \qquad i \geq 1 \tag{50}$$

is consistent with the well-known result for linear white, Gaussian forcing

$$\phi(\omega) = |\hat{K}^1(\omega)|^2 \tag{51}$$

Successive moment expansions arising from (41) or (42) become progressively more complicated. For example, the skewness (or bi-spectrum) -- truncated to second order terms is given by

$$\overline{\hat{u}(\omega_1)\,\hat{u}(\omega_2)\,\hat{u}^*(\omega_1+\omega_2)} = 4\pi\,\hat{K}^1(\omega_2)\Big\{\hat{K}^1(\omega_1)\,\hat{K}^{2\,*}(\omega_1,\omega_2)$$
$$+\,\hat{K}^1(\omega_1)\,\hat{K}^{1\,*}(\omega_1+\omega_2)\,\hat{K}^2(-\omega_1,\omega_1+\omega_2)$$
$$+\,\hat{K}^2(-\omega_1,\omega_1+\omega_2)\,\hat{K}^1(\omega_1)\,\hat{K}^{1\,*}(\omega_1+\omega_2) \qquad (52)$$
$$+\,\frac{1}{\pi}\int\Big[\hat{K}^2(\omega_1-p,p)\,\hat{K}^2(\omega_1+\omega_2-p,p-\omega_1)\,\hat{K}^{2\,*}(p,\omega_1+\omega_2-p)$$
$$+\,\hat{K}^2(\omega_2-p,p)\,\hat{K}^2(\omega_1+\omega_2-p,p-\omega_2)\,\hat{K}^{2\,*}(p,\omega_1+\omega_2-p)\Big]\Big\}dp + \ldots$$

Equation 52 indicates several other features of the W-H representation. In general, a description of turbulence with an infinity of moments is equivalent to a description with an infinity of kernels. Also higher moments representing the non-Gaussian structure are characterized by interactions between the K^i, or equivalently among a hierarchy of non-linearities. It is possible, at least in principle, to recover one set of statistics from another by solving the (infinite) set of coupled integral equations.

Some simplification is obviously needed. The truncation of the W-H expansion is yet another case in which the closure problem of turbulence must be faced. Attempts to determine the kernels dynamically (Meecham and Siegel, 1964) have been shown to be inappropriate (Orszag and Bissonnette, 1967). Attempts to produce the equivalent of a stimulation technique (George, 1959; Dutton, 1970) and correlate the input and output are not applicable. The method of Robinson (1967a,b) based on Wiener's original work as a method of determining the kernels of a linear (or equivalent linear) system, by predictive decomposition is unwieldly and time consuming. The next section outlines a method of solving for K^1 for a generalized class of spectra which is compact and computationally efficient.

4. Spectral Factorization

As a demonstration of the basic features of spectral factorization, consider the first order linear system driven by white noise defined by the differential equation

$$\frac{dy(t)}{dt} + T^{-1}\, y(t) = \xi(t) \tag{53}$$

where $y(t)$ is the response to the white noise $\xi(t)$, and T characterizes the response time. For convenience, let us scale the problem so that $T = 1$. This equation is often employed (for example, Skelton, 1968) to describe aircraft response to turbulence. The solution of (53) is given by

$$y(t) = \int_0^\infty e^{-t_1}\, \xi(t-t_1)\, dt_1 \tag{54}$$

The kernel, K^1, is given by e^{-t}, for $t > 0$. The Fourier transform of (53) is

$$\hat{y}(i\omega-1) = \hat{\xi} \tag{55}$$

or, from (33)

$$\hat{K}^1(\omega) = (i\omega-1)^{-1} \tag{56}$$

The spectrum follows from (56) -

$$\begin{aligned} \phi_y(\omega) = \overline{\hat{y}\,\hat{y}^*} &= \hat{K}^1\, \hat{K}^{1*} \\ &= (i\omega+1)^{-1}\, (-i\omega+1)^{-1} \\ &= (\omega^2+1)^{-1} \end{aligned} \tag{57}$$

The spectral factorization problem is the inverse problem. Given the spectrum, ϕ_y, and the fact it was derived from a white, Gaussian stationary process, find $\hat{K}^1$ and K^1. In the above example the spectral factors, $1+i\omega$ and $1-i\omega$, are well-known and derivable analytically in several ways. In fact, applications with this spectrum (often referred to as a Dryden spectrum) have been made simply to utilize the known spectral factors and simple form of the kernel (even though it is known that the turbulence spectrum varies as $\omega^{-5/3}$. Such an assumption is useful because the analytical determination of the factors of other spectra, such as von Kármán's spectrum, is analytically prohibitive.

The determination of $\hat{K}^1$ from ϕ_y is not a unique process, as the problem is stated above. There are an infinity of functions, y(t), which one could find which would have the property

$$\overline{\hat{y}\,\hat{y}^*} = \hat{K}^1\,\hat{K}^{1\,*} = \phi_y \tag{58}$$

It is necessary therefore to distinguish $\hat{K}^1$ from any other $\hat{y}$ which has the same spectrum.

The defininig characteristics of $\hat{K}^1$ and $\hat{K}^1$ can be seen by considering a simpler problem where the input is a single pulse,

$$\xi(t) = \delta(t). \tag{59}$$

From (54) the output response is

$$y(t) = K^1(t) \qquad (t > 0) \tag{60}$$

that is, the kernel function is the response for a single pulse. (Consequently, $\hat{K}^1$ is referred to, in what follows, as a kernel or a response function.) The function, K (t), of (60) is, from (54)

$$\begin{aligned} K^1(t) &= e^{-t} \qquad t \geq 0 \\ &= 0 \qquad\quad t < 0 \end{aligned} \tag{61}$$

so that for a pulse $(\delta(t))$ at $t = 0$, the response is instantaneously at its maximum after the impulse begins. This property is referred to as the minimum phase or delay characteristic, because the modeled physical system responds with the minimum possible delay to a change in the input. Physically, of course, a finite delay would be required before the system achieved its maximum response. It is noted that the modeled process (53) is free from frictional and inertial effects which we would expect intuitively to delay the initial response.

The spectral factorization process using the minimum delay criterion was also shown by Bode and Shannon (1950) to be equivalent to determining a function with a given modulus (spectrum) with zeroes confined to one half of the complex plane. The general factorization problem was solved by Kolmogorov and is discussed in detail by Doob (1953).

In what follows, the development is heuristic. Also, because the remaining development and computations will necessarily be in discrete, tabulated form, the formulation is given in an equivalent, discrete representation. That is, $\hat{K}$ (dropping the super-script 1 for convenience) is redefined as

$$\hat{K}(\omega) = \sum_{t=0}^{\infty} k_t \, e^{i\omega t} \tag{62}$$

where k_j is the kernel tabulated over the index t and the summation limits reflect the condition that

$$k_i = 0 \qquad i < 0 \tag{63}$$

The phase characteristic, $\psi(\omega)$, of the Fourier transform of the kernal, is defined by

$$\hat{K}(\omega) = \phi^{1/2}(\omega) \, e^{i\psi(\omega)} \tag{64}$$

Consider a Fourier transformation of the logarithm of $\hat{K}$, given by

$$\begin{aligned} \ln \hat{K} &= \sum_{t=0}^{\infty} L_t e^{i\omega t} \\ &= L_o + \sum_{t=1}^{\infty} L_t \cos \omega t + i \sum_{t=1}^{\infty} L_t \sin \omega t \end{aligned} \tag{65}$$

The one-sided nature of (65) results from the equivalence of the physical realizability condition on K (63) and the lack of poles in the lower half plane (complex) of frequency (Robinson, 1967a). The integration (65) is equivalent to evaluating singularities in the upper half plane only. The Fourier transform of $\ln \phi^{1/2}$ is given by

$$\ln \phi^{1/2} = \alpha_o + 2 \sum_{t=1}^{\infty} \alpha_t \cos \omega t \tag{66}$$

where the symmetric nature of the spectrum alters the range of summation. Accordingly, the coefficients, α, are derived from the inverse transform of $\ln \phi^{1/2}$,

$$\alpha_t = \frac{1}{2\pi} \int_{-\pi}^{\pi} \cos \omega t \ln \phi^{1/2}(\omega) \, d\omega \tag{67}$$

From (67), by forming logarithms of both sides, we have

$$\begin{aligned} \ln \hat{K}(\omega) &= L_o + \sum_{t=1}^{\infty} L_t \cos \omega t + i \sum_{t=1}^{\infty} L_t \sin \omega t \\ &= \alpha_o + 2 \sum_{t=1}^{\infty} \alpha_t \cos \omega t + i\psi(\omega) \end{aligned} \tag{68}$$

By equating coefficients in cos ωt and sin ωt we are led to

$$L_o = \alpha_o \tag{69}$$

$$L_t = 2\alpha_t \quad \text{for } t > 0 \tag{70}$$

The phase $\psi(\omega)$ in (64) essentially selects a function $\hat{K}$ with no singularities in the lower half plane. The particular phase relationship is given by

$$\begin{aligned}\psi(\omega) &= \sum_{t=1}^{\infty} L_t \sin \omega t \\ &= 2 \sum_{t=1}^{\infty} \alpha_t \sin \omega t\end{aligned} \tag{71}$$

Equation 71 is the essential result of spectral factorization. It states that the phase characteristic that distinguishes the kernel from any other function with spectrum ϕ can be computed in terms of the spectrum itself. This result is clear if we substitute (67) into (71) to produce

$$\psi(\omega) = \frac{2}{\pi} \sum_{t=1}^{\infty} \sin \omega t \int_0^{\pi} \cos \omega_1 t \ln \phi^{1/2} (\omega_1) \, d\omega_1 \tag{72}$$

The class of spectra to which such an operation will apply depends on whether the spectrum obeys the Paley-Wiener condition

$$\int_{-\infty}^{\infty} \frac{\ln \phi(\omega)}{(1+\omega^2)} \, d\omega > -\infty \tag{73}$$

This constraint is discussed in (Kerman, 1965, Appendix B) as it relates to numerical approximations.

5. Model of the Vertical Velocity

The importance of the vertical velocity spectra, both in modeling the response of aircraft to turbulence and in studying the vertical flux of momentum and heat near the earth's surface, is indicated by the availability of empirical estimates of its spectral form. Busch and Panofsky (1968) have approximated the w spectra (normalized by u_*^2) by a form

$$f\, G_w(f) = \frac{A_w f}{1+B_w f^{5/3}} \tag{74}$$

based on data drawn from several sites (f is defined in (9)). They note that at low wave numbers, $f < 1$, their empirical form is an improvement over that suggested by Pasquill and Butler (1964),

$$f\, G_w(f) = \frac{A_w f}{(1+B_w f)^{5/3}} \tag{75}$$

Confirmation of the Busch-Panofsky form is supplied by Kaimal et al. (1972) based on the Kansas data. However, the estimates for (A_w, B_w), for neutral stability, vary between the estimates of Kaimal (1.0,1.5) and Busch and Panofsky (1.5,2.7). The variation in these coefficients is indicative of the accuracy that can be expected in estimating characteristics associated with spectra, such as variance, length scale, dissipation, and response functions. All empirical spectra behave asymptotically as $f^{-5/3}$, which is characteristic of the Kolmogorov region ($1 \ll f \ll f_{KOL}$).

Another spectral form

$$f\, G_w(f) = \frac{A_w \phi_\varepsilon^{2/3} f^{2/3}}{1+(B_w f)^{4/3}} \tag{76}$$

is convenient mathematically but does not have the usual front slope of +1 found by observations. The convenience of (76) lies in its form after a transformation of variables

$$f' \sim f^{2/3} \tag{77}$$

From the invariance of energy with a change of variables

$$f\, G_w = f'\, G'_w \tag{78}$$

we are led to

$$f'\, G' \quad \frac{f'}{1+(B'_w\, f')^2}$$

which is a form familiar in filtering problems and which has a well-defined kernel for a linear response to white noise given by

$$\begin{aligned} K^1(x') &= \exp - x'/B'_w \qquad x' > 0 \\ &= 0 \qquad\qquad\quad x' < 0 \end{aligned} \tag{80}$$

Because (77) is related to a transformation of the space variables

$$x' \sim x^{2/3} \tag{81}$$

the general form of the response function is expected to be

$$K^1(x) = \gamma_w{}^{1/2} \exp -(x/B_w)^{2/3}\, H(x/B_w) \tag{82}$$

where the function H carries the effect of the linear Fourier transformation involved in factoring (79) to obtain (82). The coefficient γ_w can be shown to be

$$\begin{aligned} \gamma_w &= A_w\, \phi_\epsilon{}^{2/3}\, B_w{}^{-2/3} \\ &= \frac{4}{3\pi}\, \overline{\tilde{w}^2} \end{aligned} \tag{83}$$

The response function of any empirical formulation for w spectra, to the extent that it approximates (76), can be expected to vary according to (82). Therefore, it is useful to examine the basic structure of response functions in (82) for H = 1.

a) Analytical Characteristics of Response Structure

The form of the approximate analytical kernel is shown in Figure 1, both as a function of scale distance and of stability, where the parameter ζ is defined in (6). The variation of $\gamma_w^{1/2}(\zeta)$ and $B_w(\zeta)$ is based on the empirical relations drawn from the Kansas field experiment and is given in Figure 2. The general feature of the solution for K^1 is a monotonic decrease of the response with distance (in the direction from which the turbulence is advected). The kernel for separations less than $\ell(\tilde{x} < 1)$ decrease faster than exp $(-\tilde{x})$ but decreases less rapidly than the response of a simple linearly damped system for $\tilde{x} > 1$. That is, the approximate analytical solution, $\exp(-\tilde{x}^{2/3})$, indicates a decrease in the response for small time lags (relative to ℓ/u_*), or equivalently, indicates that the filter will give less weight to the more immediate past. On the other hand, the response for large largs will be greater than that for the common first order linear model.

The effects of stratification on the kernel, also given in Figure 1 are two-fold. First, the initial response ($\tilde{x} = 0$) varies with stability and is a minimum in neutral conditions. Second, the rate of decay of response decreases with decreasing stability. The minimum initial response is a reflection of the minimum in $\overline{\tilde{w}^2}$ at $\zeta = 0$. The rate of decrease of K^1 is determined by B_w. For increasing instability (Figure 2), B_w increases as more energy is introduced at larger f (Lumley and Panofsky, Chapter 5) and from (82), the response at a given $\tilde{x}$ also increases.

Another concept which can be demonstrated for the simple analytical approximation is the memory of the system. Intuitively, memory may be considered as the integrated effect of past stimuli. For convenience, it is desirable to compare the memory of the process representing turbulence with that of a simple linear first order process with the same variance. Memory is defined tentatively as

$$\begin{aligned} \text{Mem} &= \left\{\int_0^\infty K^1(y)\ dy\right\} \Big/ \left\{K^1(0) \int_0^\infty \exp(-y)dy\right\} \\ &= \frac{1}{K^1(0)} \int_0^\infty K^1(y)\ dy \end{aligned} \tag{84}$$

It is noted that this definition is only useful if $K^1(0) \neq 0$. For the kernel (82), Mem $\approx$ 1.33, which indicates a net increase in memory of about 0.33 relative to a simple first order process. For a slightly different version of the memory concept, given by

$$\text{Mem}(\tilde{x}) = \frac{1}{K^1(0)} \int_0^{\tilde{x}} K^1(y)\ dy \tag{85}$$

the memory as a function of distance or time from a stimulus is itself a function of scale. From Figure 1, $\text{Mem}(\tilde{x}) < 1$, for $\tilde{x} > 1$. Therefore the increased total memory which is greater than unity $\left(\text{Mem}(\infty) = 1.33\right)$, results from the large scale structure of K^1.

b) Kernels of Empirical Spectra

The spectral factorization procedure was applied numerically to some of the empirical spectral representations of Busch and Panofsky, Kaimal et al., and Pasquill and Butler as well as the spectrum in the previous section. The objective was to determine the range of response estimates which could be expected from variations in empirical representations of the w spectra. This variability provides a realistic estimate of accuracy against which to contrast other sources of variability, such as arise in the parameterization of the thermal stability.

The kernel K^1 obtained by factorization of some of the empirical spectra are given in Figure 3. Also shown are the results for K^1 arising from the common spectral form used by Busch and Panofsky and Kaimal et al., but with A_w and B_w altered for compatability with the variance and Kolmogorov range structure. The final kernel plotted in Figure 3, and termed "model", corresponds to the spectral form $f^{-1/3}(1+B_w f)^{4/3})^{-1}$, with coefficients chosen for compatability with the variance and inertial range structure.

The response function, as expected, is monotonic and similar to the basic exp $(-\tilde{x}^{2/3})$ form of the previous section. It is noted that estimates of K^1 using the Busch-Panofsky formulation differ significantly with increasing scale from either of the formulations based on the Kansas data. The response based on the Kansas data for $\tilde{x} > 1$ is not as large as the kernel derived from the Busch-Panofsky data. The variance compatible spectrum, based on the common mathematical form used by both Kaimal et al. and Busch and Panofsky, results in a response structure markedly different from the Busch-Panofsky form alone. It is concluded that the normalized variance characteristics of the data set drawn from the Kansas experiment and that used by Busch and Panofsky differ significantly.

The underlying reasons for this disparity are not clear, but may be attributed to some degree to the larger roughness characteristic of the Busch-Panofsky data set, or perhaps a difference in similarity involving the average structure of the large scale flows (Kerman, 1974b). Whatever the cause of the disparity in the form of K^1, the results indicate that a significant difference exists in the response representation at scales, $\tilde{x} > 1$, resulting from various experiments. From Figure 1, the estimated errors between the function forms are about equivalent to an error of $\pm$ 0.25 in an estimate of ζ. The numerical estimate of the kernel corresponding to the model spectrum underestimates the small scale response and overestimates the large scale response. An examination of the different spectra factored to produce the response estimates (Figure 4) reveals the close relationship that exists between the relative distributions of variance of the spectra and the relative response structures. For spectra with additional variance at scales, $f < 1$, (for example, the analytical model spectrum) the result is an increased response at scales, $\tilde{x} > 1$, and vice versa.

c) Stratification Effects on Kernels

Alternatively, the function, K^1, can be described by two of its characteristics -- its initial response at $\tilde{x} = 0$, and its integral, or memory. The function $K^1(0)$ and its memory is displayed in Figure 5 as a function of ζ, for the particular model described in Section b. The calculations in the spectral factorization are performed with 128 points in the Fast Fourier Transform (FFT) algorithm. The response at $\tilde{x} = 0$ differs from that of Figure 2 because of the approximations made near f_{max} (Kerman, 1975, Appendix B).

In Figure 5, the initial response increases with $|\zeta|$ and the memory increases monotonically with increasing instability. The response function implied in Figure 5 is equivalent to that shown in Figure 1. The response for a given $\tilde{x} > 0$ is less for stable stratification than for unstable stratification and a minimum for neutral stability. The structure of the response function, normalized by its initial value, also follows from qualitative consideration of the change in the spectra with stratification. While the variance, $\overline{\tilde{w}^2}$ (which in (83) determines the initial response) increases in both stratifications, the spectral bandwidth, B_w, (which determines the decay rate of response) increases monotonically with decreasing stability. Accordingly, the excitement of more large-scale energy results in an increased response at scales $\tilde{x} > 1$.

It follows from the scaling of the spectra that the response for an arbitrary stability, scaled by its initial response, is only a function of $\tilde{x}/B_w$. For a constant flux layer in which the Monin-Oboukhov length, L, is also constant with height, one may equate changes in $\zeta(= z/L)$ with changes in height. Therefore, for a given x, $\tilde{x}/B_w$ will decrease with height, both because $\tilde{x}(= x/\ell)$ decreases with height and because B_w^{-1} decreases with height (Figure 2). Accordingly, the response will increase as a result of an increase in $\overline{\tilde{w}^2}$ with height and a decrease in $\tilde{x}/B_w$ with height. Under stable conditions, B_w increases approximately linearly with height, as does $\gamma_w^{1/2}$, so that from (82), for a given x,

$$K^1(z) \sim z \exp(- z^{-4/3}) \qquad (86)$$

Under stable conditions, B_w is approximately constant, while $\gamma_w^{1/2}$ again varies linearly with height, so that for a given x,

$$K^1(z) \sim z \exp(- z^{-2/3}) \tag{87}$$

For neutral conditions, both $\gamma_w^{1/2}$ and B_w are constants in height, and the response function has a form

$$K^1(z) \sim \exp(- z^{-2/3}) \tag{88}$$

For large enough z, assuming $\kappa z/\ell$ is still nearly unity, the response, for a given x, will vary linearly with height in stratified cases and approach a constant in neutral cases.

d) Predictive Structure of the Model

In the development of control systems it is advantageous to be able to predict the turbulent velocity field at some future time, on the basis of past observations. In order to be able to apply some properties of linear stochastic processes to the linear, Gaussian model of the vertical velocity component, it is necessary to examine another property of response functions. An inverse linear functional, K^{-1}, is defined by

$$\int K(t_1)\, K^{-1}(t-t_1)\, dt_1 = \delta(t) \quad . \tag{89}$$

A Fourier transformation of (89) produces an equivalent definition

$$\hat{K}(\omega)\, \hat{K}^{-1}(\omega) = 1 \tag{90}$$

Accordingly, the inverse linear functional is derivable from the kernel, K, by the method implied in (89) or (90). For a perfect system, without noise, the inverse functional generates a white, Gaussian process, ξ, from a shaped spectral process, w, in the manner

$$\xi(t) = \int K^{-1}(\tau)\, w(t-\tau)\, d\tau \tag{91}$$

Let us consider a prediction of w in terms of its filtered past. The filter is determined so as to minimize the least squares error between the prediction and verification (Robinson, 1967b). The linearly predicted value, $w_p(t+\alpha)$, at a time α in the future is given by

$$w_p(t+\alpha) = \int M(\tau;\alpha)\, w(t-\tau)\, d\tau \tag{92}$$

For a linear W-H representation of w (Robinson, 1967b), the prediction kernel, M, is given in terms of K and K^{-1} by the expression

$$M(\tau;\alpha) = \int K(p+\alpha)\, K^{-1}(\tau-p)\, dt \tag{93}$$

From (89) or (90), Equation 93 can be considered as a relationship between M and K.

The inverse filter K^{-1} computed from the kernel of the analytical spectral model, under neutral, inviscid conditions, is given in Figure 6. The physical effect of K^{-1} is to filter a correlated time series to produce a white noise process. In Figure 6, this decoupling of the time series is accomplished by the alternate oscillating weights near $\tilde{x} = 0$ in what amounts to a shredding action. A measure of the effect of an inverse filter therefore lies in the difference $K^{-1}(0) - K^{-1}(\Delta\tilde{x})$, where $\Delta\tilde{x}$ is the resolution for the white noise process which will be generated. The larger the difference, the more the necessary shredding action to destroy the turbulent correlations. Accordingly, for situations with different spectral bandwidth in different thermal stabilities the oscillations in K^{-1} near $\tilde{x} = 0$ will increase for decreased stability.

The results for the prediction kernel, M, are given in Figure 7 for several values of $\alpha\Delta\tilde{x}$. The most distinctive feature of the structre of M is the very rapid decrease in predictive weighting even for $\tilde{x} < 0.25$. The implication is that the best estimate (in the least squares sense) of w at a distance $\alpha\Delta\tilde{x}$ ahead is given effectively as a multiple of its present value. The error of a prediction $\alpha\Delta\tilde{x}$ units ahead is given by

$$\Sigma^2(\alpha\Delta\tilde{x}) = \left|\tilde{w}(\tilde{x} + \alpha\Delta\tilde{x}) - \tilde{w}_p(\tilde{x} + \alpha\Delta\tilde{x}\right|^2$$

$$= 1 - \int M(r\Delta\tilde{x}, \alpha\Delta\tilde{x})\ \overline{\tilde{w}^2}\ \left((\alpha+r)\ \Delta\tilde{x}\right)\ d(r\Delta\tilde{x}) \qquad (94)$$

Intuitively, the rate of growth of error Σ^2, with distance into the future, is a measure of the predictability of the turbulent process simulated by the linear representation.

The error of prediction of the analytical model is given in Figure 8. The deterioration of the prediction at even short distances is apparent. For example, at $\alpha\Delta\tilde{x} = 0.5$, $\Sigma^2(0.5) \approx 0.6$, or $\Sigma \approx 0.8$. That is, at a distance of about $\ell/2$, the root mean square error in estimating the vertical velocity will be about 80 percent of $\overline{w^2}^{1/2}$. For comparison, a test was conducted on the common first order linear process, with comparable bandwith. The results are shown also in Figure 8. A comparison of the mean square error Σ^2 of the turbulent spectral model ($f^{-5/3}$) and the common first order model (f^{-2}) indicates a modest improvement in predictability at scales comparable to ℓ. It is concluded on the basis of this comparison that modeled turbulence is the more predictable process. This result is also in agreement with the previous discussion of the memory of the simulated turbulence.

e) Empirical Formulae for Simulation

In the discussion on analytical characteristics, the filter for simulation purposes was represented in the form

$$K^1(\tilde{x}) = \gamma_w^{1/2} \exp-(\tilde{x}/B_w)^{2/3}\ H(\tilde{x}) \qquad (95)$$

For the purpose of application of the model, it is convenient to summarize the forms γ_w, B_w and H.

The factor $H(\tilde{x})$ was computed from numerical results for K^1 for various stabilities, ζ, using the following empirical formulae for γ_w and B_w

$$\gamma_w^{1/2} = 0.75\ (1 + 0.75|\zeta|) \qquad (96)$$

$$B_w = 0.7\ (1 + 0.75\ \zeta + 3.0\ \zeta^2) \qquad (97)$$

over the range $-1.5 < \zeta < 0.5$. The results from $H(\tilde{x})$ for the extremes of the stability range, are shown in Figure 9. Apparently, H is only a weak function of the bandwidth, B_w, of the spectrum used. Accordingly, stability effects are ignored in approximately H. The form chosen to represent H empirically is given by

$$H(\tilde{x}) = 0.5\ (1 + \exp[-\ 2.5\ \tilde{x}^{2/3}]) \tag{98}$$

The specification (95) of the first order kernel of the linear, Gaussian vertical velocity model is now complete. The application of these formulae requires establishing estimates of u_* and T_* for a given height, roughness and geostrophic wind speed to denormalize the tabulated functions. An example using the resistance law formulations is given by Kerman (1974a).

6. Implementation of Model

Standard computer sub-routines exist for the generation of randomly ordered, Gaussian series. The difficulty with using these random number generators lies in their small but significant deviations from a Gaussian distribution for moments of order greater than 2. The white spectrum condition is improved iteratively by several random order shufflings of the input series.

The problem of non-Gaussianity was overcome by generating random values from the cumulative probability density function of a Gaussian process. For a Gaussian process with mean 0 and variance 1, the probability, p, that a sampled value, s, will be less than x,

$$p = Pr(s \leq x) \tag{99}$$

is given by

$$p = \mathrm{erf}(x) \tag{100}$$

The range of p is (0,1) for a domain of x $(-\infty,\infty)$. Conversely, the Gaussian distributed variable x, which occurs with probability p is given by

$$x = \mathrm{erf}^{-1}(p) \tag{101}$$

The generation of N values of x from (101) was achieved for an equispaced partition of the range of probability, p, into N increments. The limit of accuracy of the routine for the inverse error function (Abramowitz and Stegun, 1964) of $5\ 10^{-5}$ for single precision computations limits the length of generated time series to about $2\ 10^{4}$ points. Conversely, because the approximation to Gaussian moments of order greater than 2 becomes increasingly dependent on several rare large deviations, it is necessary to generate a minimum number of points to achieve approximate Gaussianity in the higher moments. The minimum then depends on the degree of accuracy desired in the moments of the filtered series. The conditions on the length of the series are less stringent for linear simulations because of a lack of interaction among moments.

Several methods are available for the evaluation of the transformation

$$y(t) = \int K^1(\tau)\ \xi(t - \tau)\ d\tau \tag{102}$$

where K^1 is the filter and ξ and y are the white and filtered series respectively. The direct evaluation of (102) by either a discrete analog or a quadrature scheme results in an additional shaping of the input spectrum in addition to the filtering by $|\hat{K}^1|^2$. Therefore, it is advantageous to utilize the Fourier transform equivalent of (102) given by

$$\hat{y}(\omega) = \hat{K}^1(\omega)\ \hat{\xi}(\omega) \tag{103}$$

The evaluation of $\hat{K}^1$ in (103) may be made in either of several ways. The first method is the direct evaluation of $\hat{K}^1$ from K. However, this method was found to be inexact in specifying the low frequency (wave number) spectral content. This error in filtering the large scales arises from the recursion involved in estimating the Laguerre coefficients (Kerman, Appendix B). A second method which is more exact involves by-passing the redundant step of computing K^1 and its Fourier transform. The method of spectral factorization results in an exact estimate of $\hat{K}^1$ directly from the given input spectrum. However, in order to accommodate the fast Fourier transform techniques it is necessary to interpolate the estimate of $\hat{K}^1$, or more correctly, its regularized spectral equivalent to equal increments of ω (or f). As a result of the spectral factorization $\hat{K}^1$ is tabulated at equal increments of u where

$$\omega = \tan u/2 \tag{104}$$

The procedure used to estimate $\hat{K}^1(\omega)$ was to interpolate the regularized spectral factors for the u derived from the inverse of (104) and then to transform the ω-space using the relationship (Rino, 1970)

$$\hat{K}^1(\omega) = \hat{g}(\omega)\ [2^{-1/2}\ (1 + \exp(-iu))]^{n+1} \tag{105}$$

where $\hat{g}$ is the so-called regularized spectral factor (Kerman, 1975, Appendix B). The interpolation scheme used to interpolate $\hat{g}$ was a third-order spline function routine. The success of this second method is guaranteed by the fact that the regularized spectral density functions are smooth, slowly varying functions of scale.

The combined error of spectral factorization to estimate $\hat{g}$ and its interpolation to estimate $\hat{K}^1$ was found by computations to be less than 10^{-3} of the modulus at a given scale. Therefore in estimating a spectrum the only discernible disparity between an input spectrum of turbulence and its simulation lies in the deviation of the white noise spectrum from unity or in its statistical variability. This non-whiteness can be eliminated in spectral comparisons by normalization of the output spectrum by the input spectrum. Figure 10 presents a comparison of the empirical and simulated spectra of vertical velocity for a total length of simulation equivalent to about 10^3 integral scales. The empirical form chosen for the spectrum of w was discussed earlier. It can be seen from Figure 10 that the Kolmogorov spectral form for $f >> 1$ has been faithfully reproduced. It is concluded that within the extremes of statistical variability expected in a single finite length of record, the spectrum of the simulated turbulence normalized by the sample white spectrum is identical to the prescribed empirical spectrum.

7. In Conclusion

We have examined the method of simulating turbulence by filtering a white noise process. The calculation of filters by digital spectral factorization of empirical spectra of surface layer turbulence eliminates the need to use spectra with known spectral factors.

A comparison of several empirical formulations, for surface layer spectra and the kernels derived from them, showed that the response structure, particularly for large scales, was sensitive to the original empiricism. A definitive formulation for the energy containing sizes of the turbulence awaits further experimentation and theoretical consolidation.

The initial response and width of appreciable response were also examined relative to the thermal stratification. Initial response of velocity, normalized by surface stress, was shown to increase in any stratification. Also, the range of response broadened with decreased stability. The simulated turbulence has a somewhat larger memory than the more common first order linear model -- a property of interest for control problems. The initial response was shown to increase with height under all stratifications, but to increase more rapidly in unstable stratifications. The predictive function of the turbulence is essentially a single "now" value, and the mean square error if prediction grows rapidly with prediction distance.

A empirical formulation of the filter for various stratifications was given which will facilitate applications with the vertical velocity component. Excellent comparison was demonstrated between empirical and simulated spectra for a carefully generated white, Gaussian input.

8. References

Abramowitz, M., and I.A. Stegun, 1964: *Handbook of Mathematical Functions*, Dover.

Arya, S.P.S., 1972: Geostrophic drag and heat transfer relations for the atmospheric boundary layer. *Quart. J. Roy. Met. Soc., 101*, 147-161.

Barrett, J.F., 1963: The use of functionals in the analysis of non-linear physical systems. *J. Electronics and Control, 15*, 567-615.

Batchelor, G.K., 1953: *The Theory of Homogeneous Turbulence*. Cambridge University Press, London.

Blackadar, A.K. and H. Tennekes, 1968: Asymptotic similarity in neutral barotropic atmospheric boundary layers. *J. Atmos. Sci., 25*, 1015-1020.

Bode, H.W. and C.E. Shannon, 1950: A simplified derivation of linear least-square smoothing and prediction. Proc. Inst. Radio Eng., 38, 417-425.

Busch, N.E. and H.A. Panofsky, 1968: Recent spectra of atmospheric turbulence. *Quart. J. Roy. Met. Soc., 94*, 132-148.

Deardorff, J.W., 1972a: Numerical investigation of neutral and unstable planetary boundary layers. *J. Atmos. Sci., 29*, 91-115.

Deardorff, J.W., 1972: Three-dimensional numerical modeling of the planetary boundary layer. Notes of the Workshop in Micrometeorology, Boston, A.M.S.

Doob, J.L., 1953: *Stochastic Processes*, Wiley, New York.

Dutton, J.A., 1970: Effects of turbulence on aeronautical systems. *Progress in Aerospace Sciences, 11*, 67-109. Pergamon Press, New York.

Frenkiel, F.N. and P.S. Klebanoff, 1967: Higher-order correlations in a turbulence field. *Phys. Fluids, 10*, 507-520.

George, D.A., 1959: Continuous non-linear systems. Unpublished Ph.D. thesis, Massachusetts Institute of Technology.

Gibson, C.H. and P.J. Masiello, 1971: Observations of the variability of dissipation rates of turbulent velocity and temperature fields. Proc. Symposium on Statistical Models and Turbulence, San Diego, 427-453.

Grant, H.L., R.W. Stewart and A.J. Moilliet, 1962: Turbulence spectra from a tidal channel. *J. Fluid Mech., 12*, 241-263.

Gurvich, A.S. and A.M. Yaglom, 1967: Breakdown of eddies and probability distributions for small-scale turbulence. *Phys. Fluids, 10,* Supplement, 59-65.

Haugen, D.A., ed., 1973: *Workshop in Micrometeorology.* American Meteorological Society.

Herring, J.R., 1966: Self-consistent-field approach to non-stationary turbulence. *Phys. Fluids, 9,* 2106-2110.

Houbolt, J.C., 1973: Survey on effect of surface winds on aircraft design and operation and recommendations for needed wind research. NASA-CR-2360, 74 pp.

Kaimal, J.C., J.C. Wyngaard, Y. Izumi and O.R. Cote, 1972: Spectral characteristics of surface-layer turbulence. *Quart. J. Roy. Met. Soc., 98,* 563-589.

Kazanski, A.B. and A.S. Monin, 1961: On the dynamical interaction between the atmosphere and the earth's surface. *Bull. Acad. Sci.,* USSR, *Ser. Geophys., 5,* 786-788.

Kerman, B.R., 1974a: An application of boundary layer similarity theories to an aircraft accident investigation. *Boundary-Layer Met., 7,* 53-63.

Kerman, B.R., 1974b: On the conversion of energy and enstrophy on the meso-scale. Proceedings of the Symposium on Atmospheric Diffusion and Air Pollution, Santa Barbara, California, pp. 41-48.

Kerman, B.R., 1975: A simulation of turbulence in the atmospheric boundary layer. Doctoral thesis, Dept. Meteorology, Penn. State Univ., 164 pp.

Kerman, B.R., 1977: Digital simulation of turbulence in the atmospheric boundary layer - II Non-linear representation. Submitted to *J. Atmos. Sci.*

Kolmogorov, A.N., 1941: Local structure of turbulence in an incompressible viscous fluid for very large Reynolds numbers. *Doklady ANSSSR, 30,* 201-305.

Kolmogorov, A.N., 1962: A refinement of previous hypotheses concerning the local structure of turbulence in a viscous incompressible fluid at high Reynolds number. *J. Fluid Mech., 13,* 82-85.

Kraichnan, R.H., 1965: Lagrangian-history closure approximation for turbulence. *Phys. Fluids, 8,* 575-598.

Liepmann, H.W., 1954: Extension of statistical approach to buffeting and gust response of wings of finite span. Douglas Aircraft Report SM 15172.

Lumley, J.L. and H.A. Panofsky, 1964: *The Structure of Atmospheric Turbulence.* Interscience Publishers. New York.

Meecham, W.C. and A. Spiegel, 1964: Wiener-Hermite expansion in model turbulence at large Reynolds numbers. *Phys. Fluids, 7,* 1178-1190.

Monin, A.S. and A.M. Oboukhov, 1954: Basic laws of turbulent mixing in the ground layer of the atmosphere. Akad. Nauk. SSSR Geofis. Inst. Trudy, 151, 163-187.

Oboukhov, A.M., 1962: Some specific features of atmospheric turbulence. *J. Fluid Mech., 13,* 77-81.

Ogura, Y., 1963: A consequence of the zero-fourth-cumulant approximation in the decay of isotropic turbulence. *J. Fluid Mech., 16,* 33-49.

Orszag, S.A. and L.R. Bissonnette, 1967: Dynamical properties of truncated Wiener-Hermite expansions. *Phys. Fluids, 10,* 2603-2613.

Parente, R.B., 1970: Nonlinear differential equations and analytic system theory. *SIAM J. Appl. Math., 18,* 41-66.

Pasquill, F. and H.E. Butler, 1964: A note on determining the scale of turbulence. *Quart. J. Roy. Met. Soc., 90,* 79-84.

Rino, C.L., 1970: Factorization of spectra by discrete Fourier transform. *IEEE Trans. Info. Sci., 16,* 484-485.

Robinson, E., 1967a: Predictive decomposition of time series with application to seismic exploration. *Geophysics, XXXII,* 418-484.

Robinson, E., 1967b: *Multi Channel Time Series Analysis with Digital Computer Programs.* Holden Day. San Francisco.

Skelton, G.B., 1968: Investigation of the effects of gusts on V/STOL craft in transition and hover. Air Force Flight Dynamics Lab., TR-68-85.

Stewart, R.W., 1951: Triple velocity correlations in isotropic turbulence. *Proc. Camb. Phil. Soc., 47,* 146-157.

Tennekes, H. and J.C. Wyngaard, 1972: The intermittent small-scale structure of turbulence: data processing hazards. *J. Fluid Mech.*, *55*, 93-103.

Tennekes, H. and J.L. Lumley, 1972: *A First Course in Turbulence.* M.I.T. Press. Cambridge.

Teunissen, H.W., 1970: Characteristics of the mean wind and turbulence in the planetary boundary layer. UTIAS Review No. 32, Univ. of Toronto, Institute of Aerospace Studies.

Volterra, V., 1930: *Theory of Functionals.* Blackie. London.

Zilintinkevich, S.S. and D.V. Chalikhov, 1968: The laws of resistance and of heat and moisture exchange in the interaction between the atmosphere and an underlying surface. *Izv. Atmos. and Ocean. Phys.*, *4*, 765-772.

Zilintinkevich, S.S., 1975: Resistance laws and prediction equations for the depth of the planetary boundary layer. *J. Atmos. Sci.*, *32*, 741-752.

Figure Captions

Figure 1. Comparison of response function ($r = 1$ and $r = 2/3$) for neutral stability.

Figure 2. Variation with thermal stability of parameters of analytical approximation to linear response function.

Figure 3. Response functions for various empirical spectra.

Figure 4. Comparison of various empirical spectra.

Figure 5. Initial response and memory for model spectrum.

Figure 6. Comparison of response and inverse response functions.

Figure 7. Prediction function for several prediction distances.

Figure 8. Comparison of mean square error of prediction for the model and Dryden form of spectrum.

Figure 9. Correction to analytical approximation of response function to model spectrum.

Figure 10. Comparison of w-component spectra for empirically specified model and simulated turbulence.

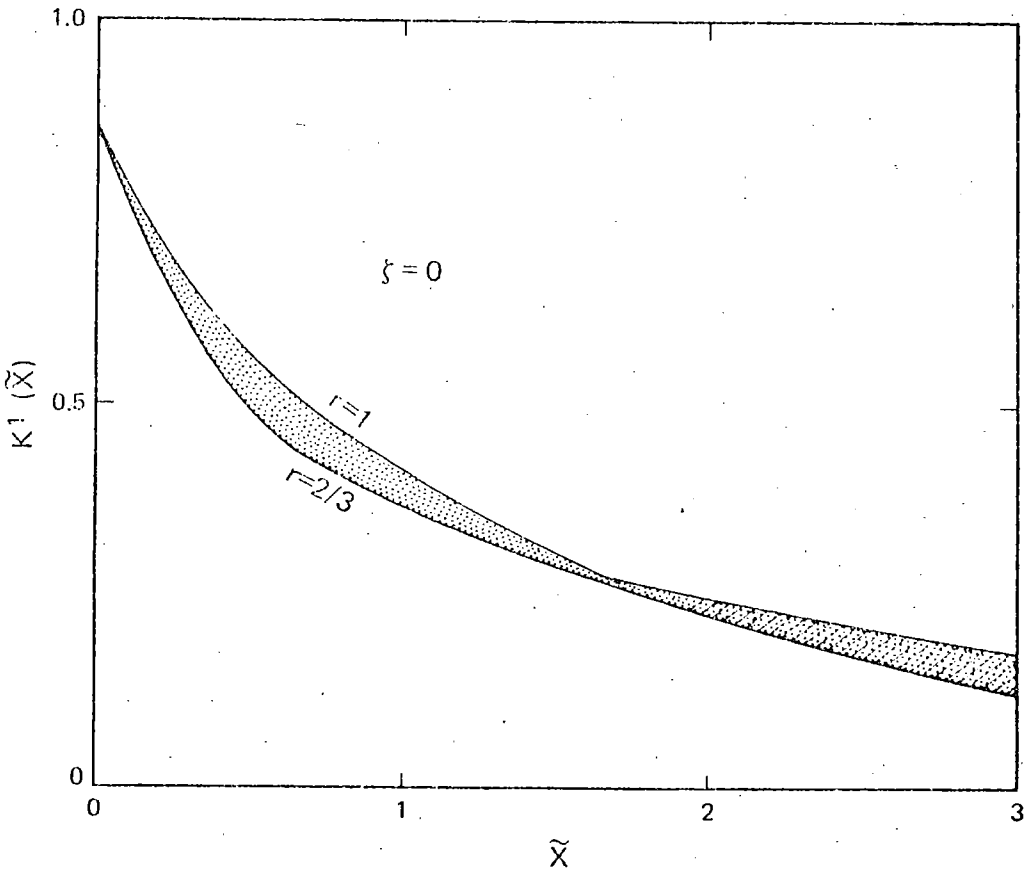

Figure 1. Comparison of response function (r = 1 and r = 2/3) for neutral stability.

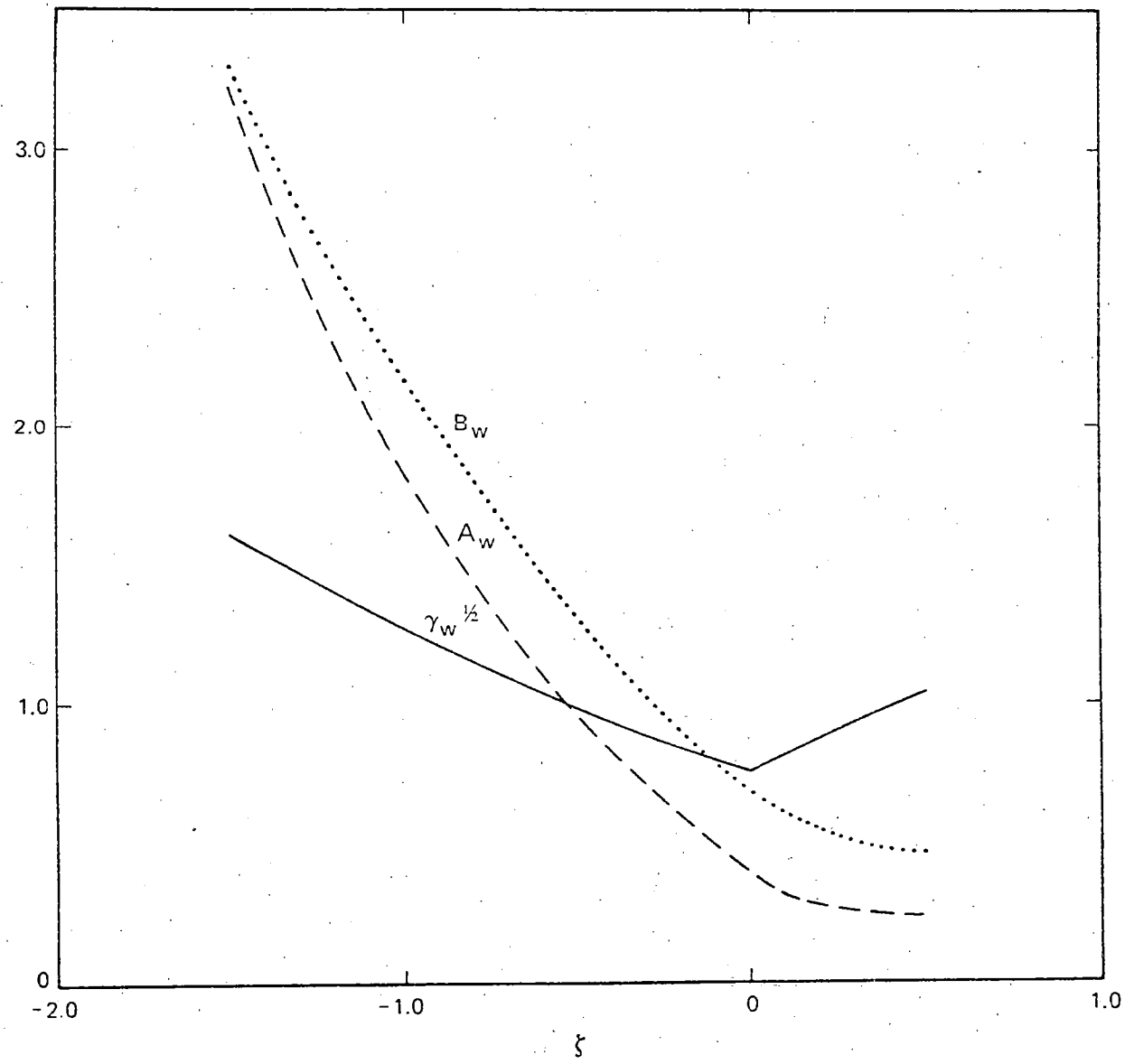

Figure 2. Variation with thermal stability of parameters of analytical approximation to linear response function.

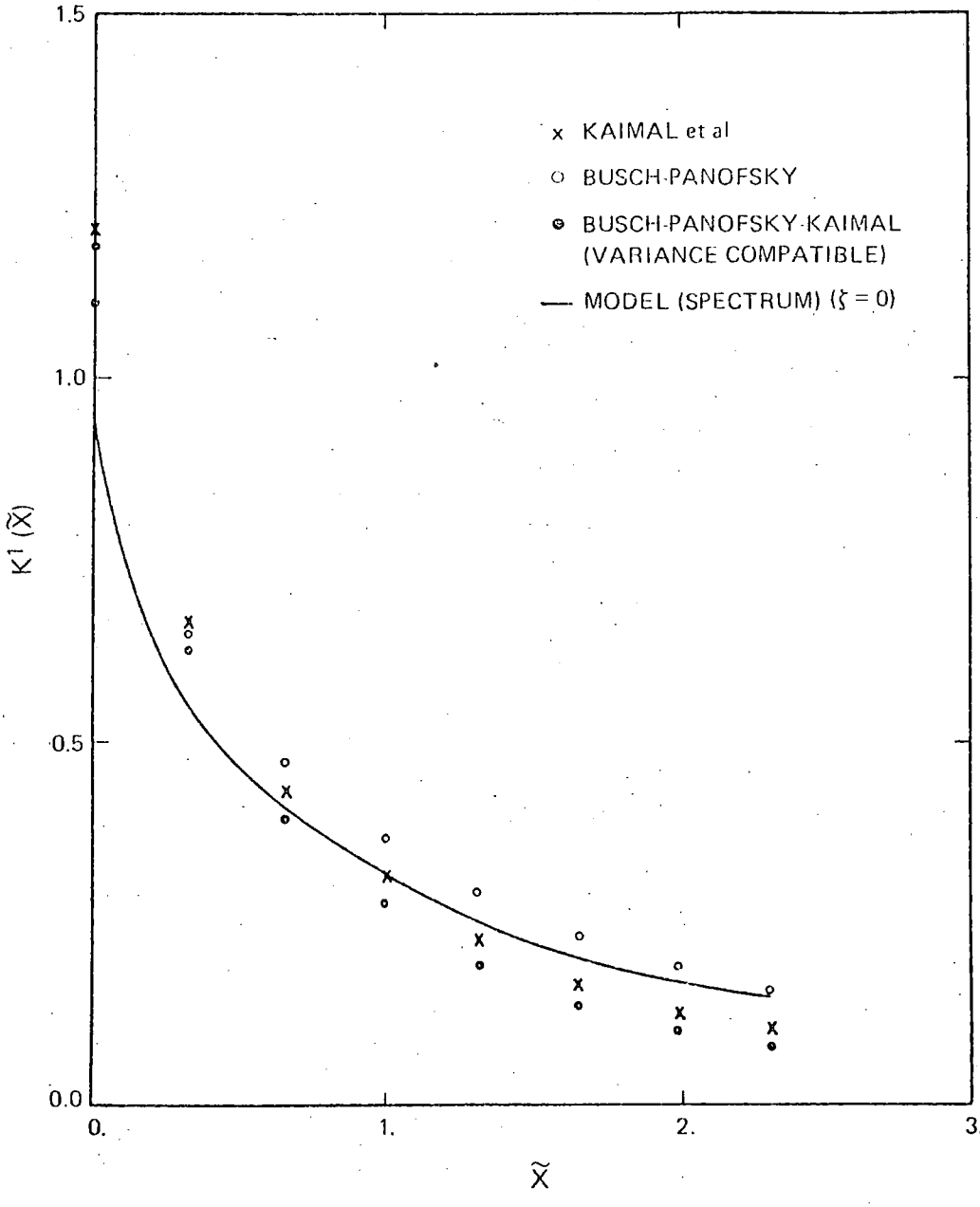

Figure 3. Response functions for various empirical spectra.

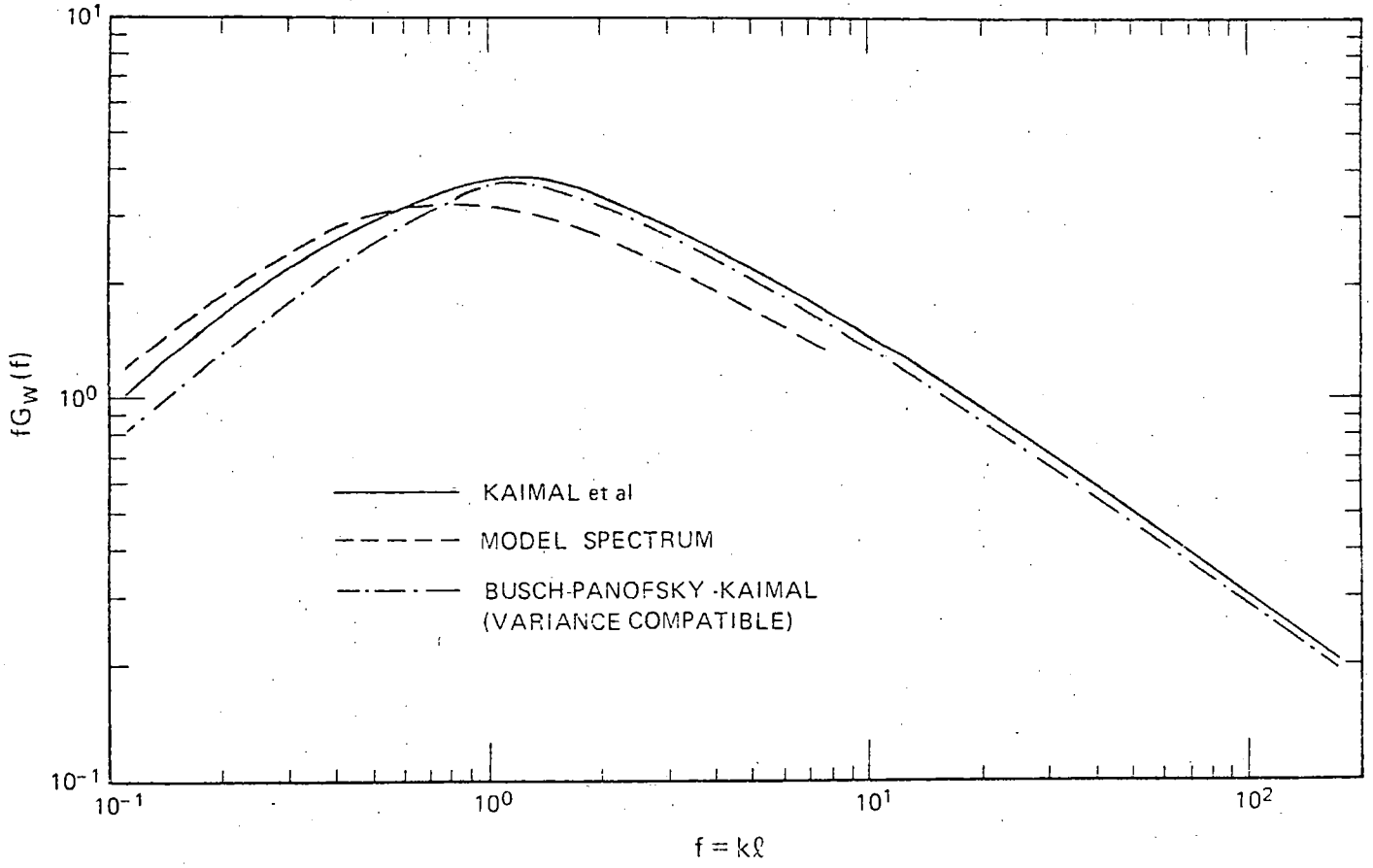

Figure 4. Comparison of various empirical spectra.

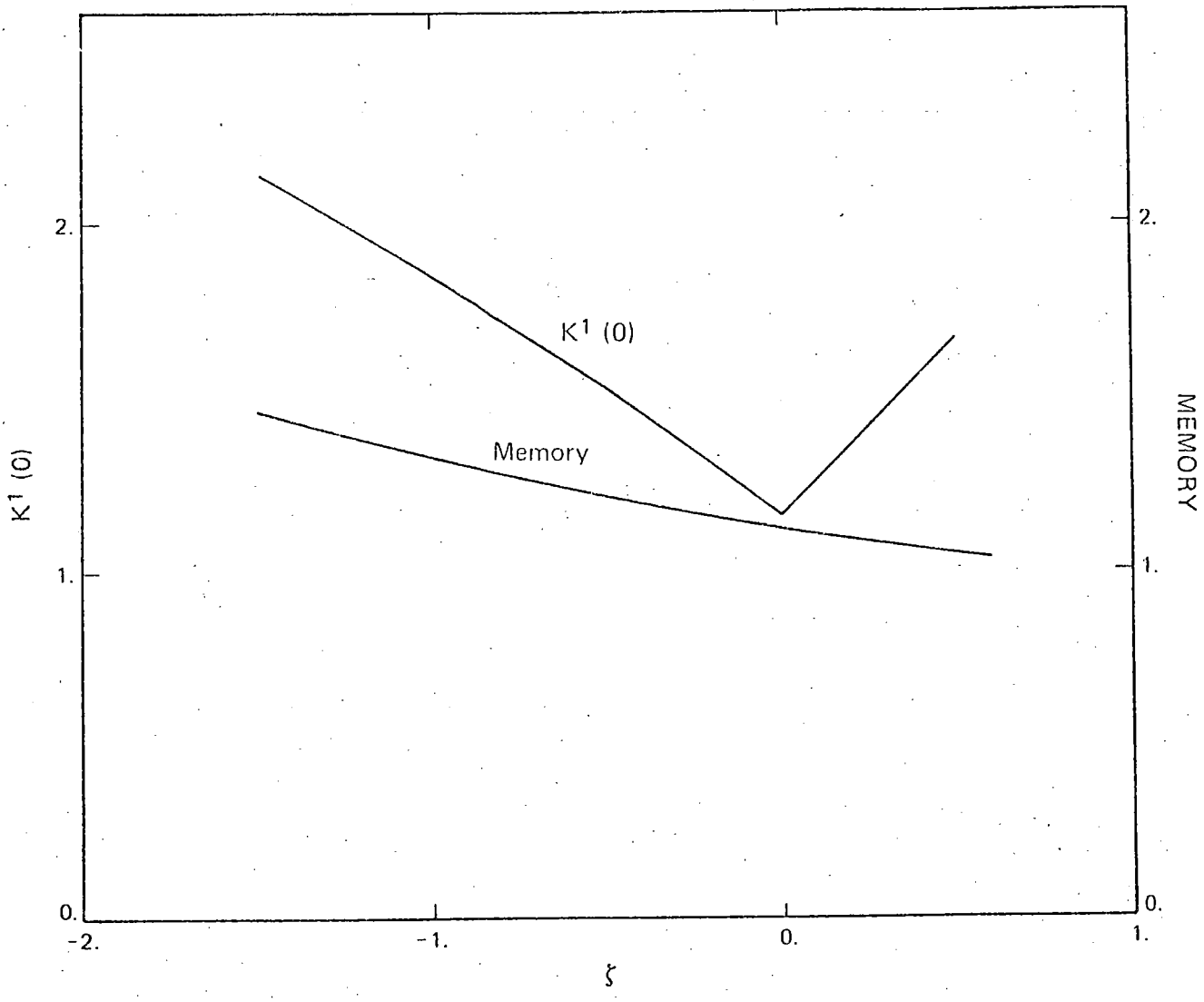

Figure 5. Initial response and memory for model spectrum.

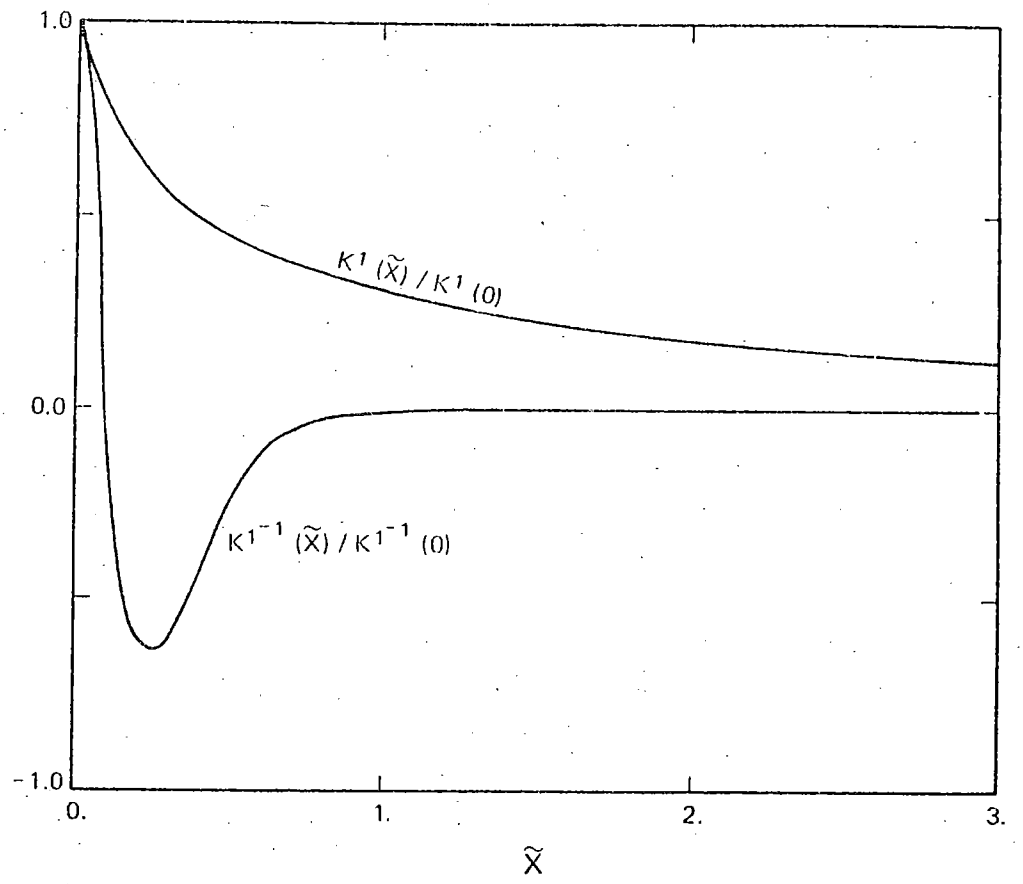

Figure 6. Comparison of response and inverse response functions.

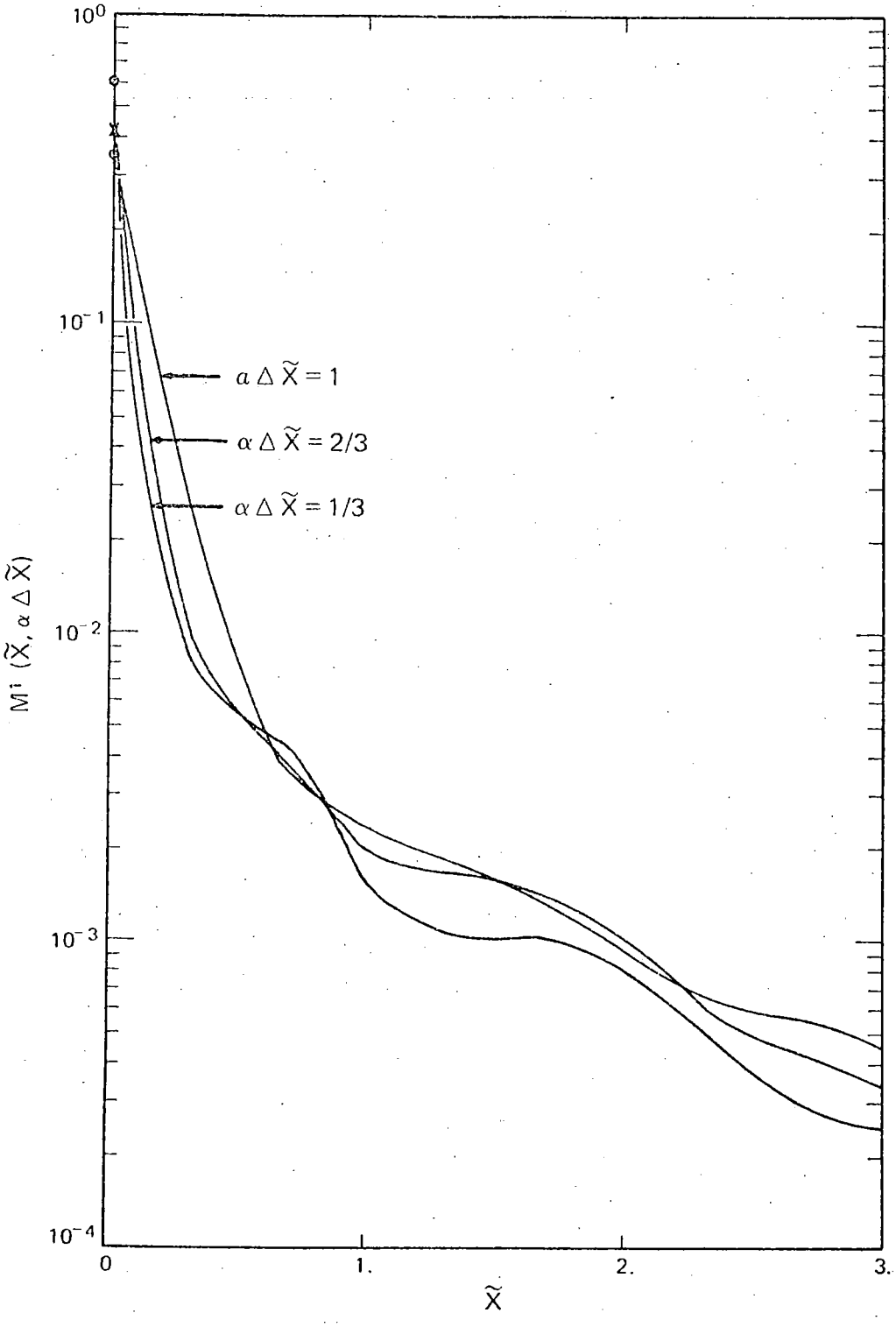

Figure 7. Prediction function for several prediction distances.

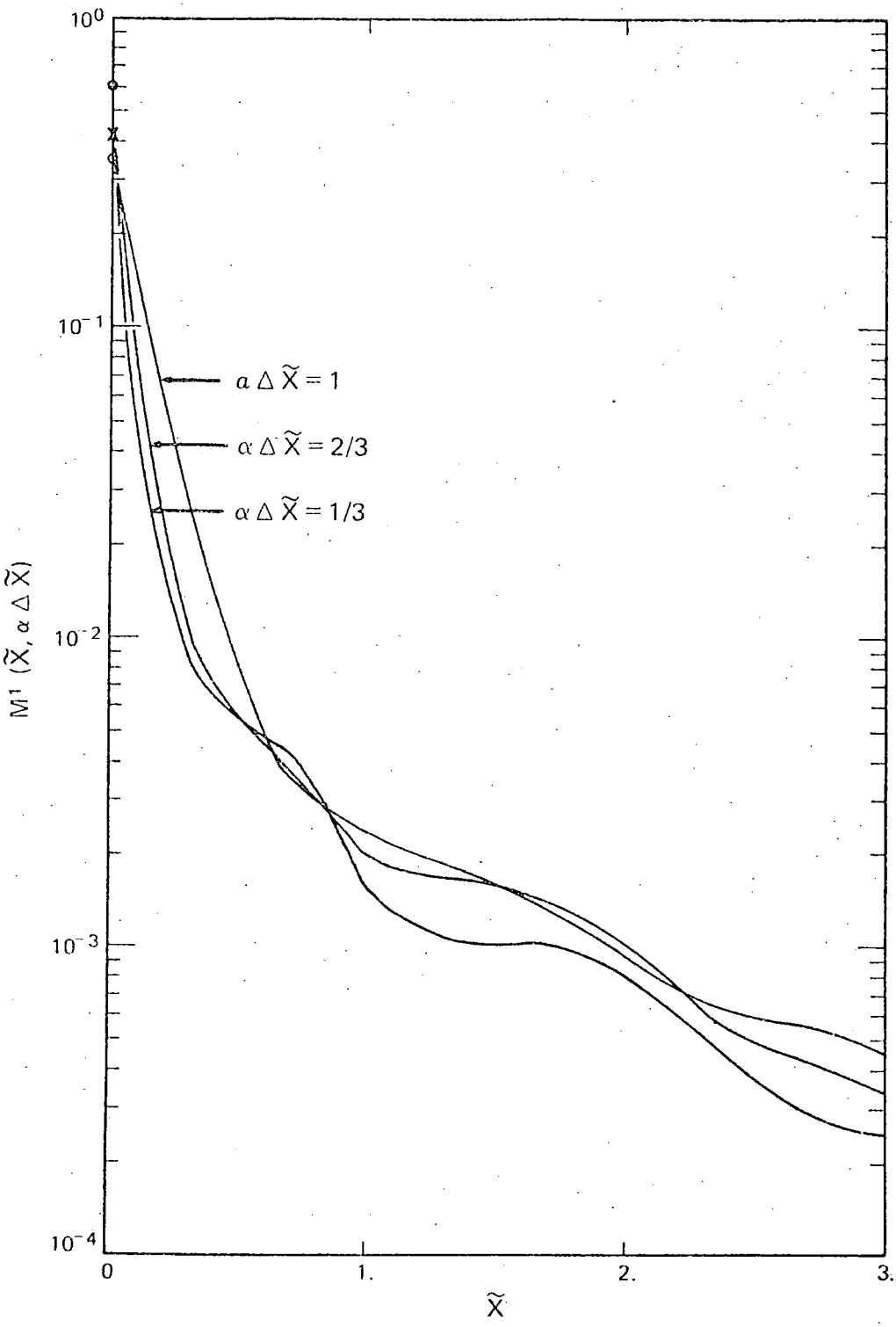

Figure 7. Prediction function for several prediction distances.

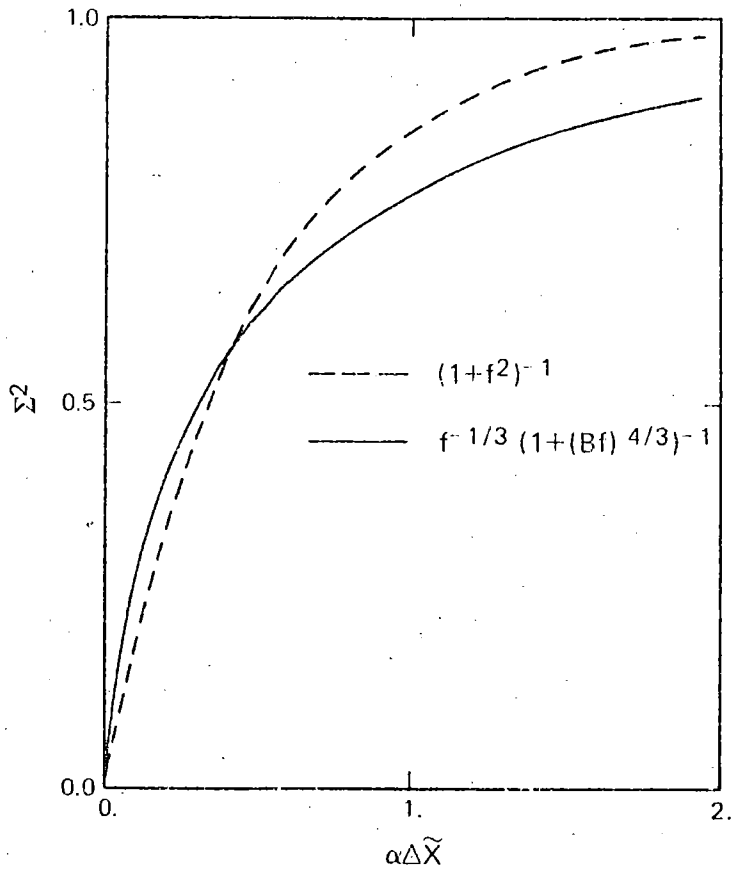

Figure 8. Comparison of mean square error of prediction for the model and Dryden form of spectrum.

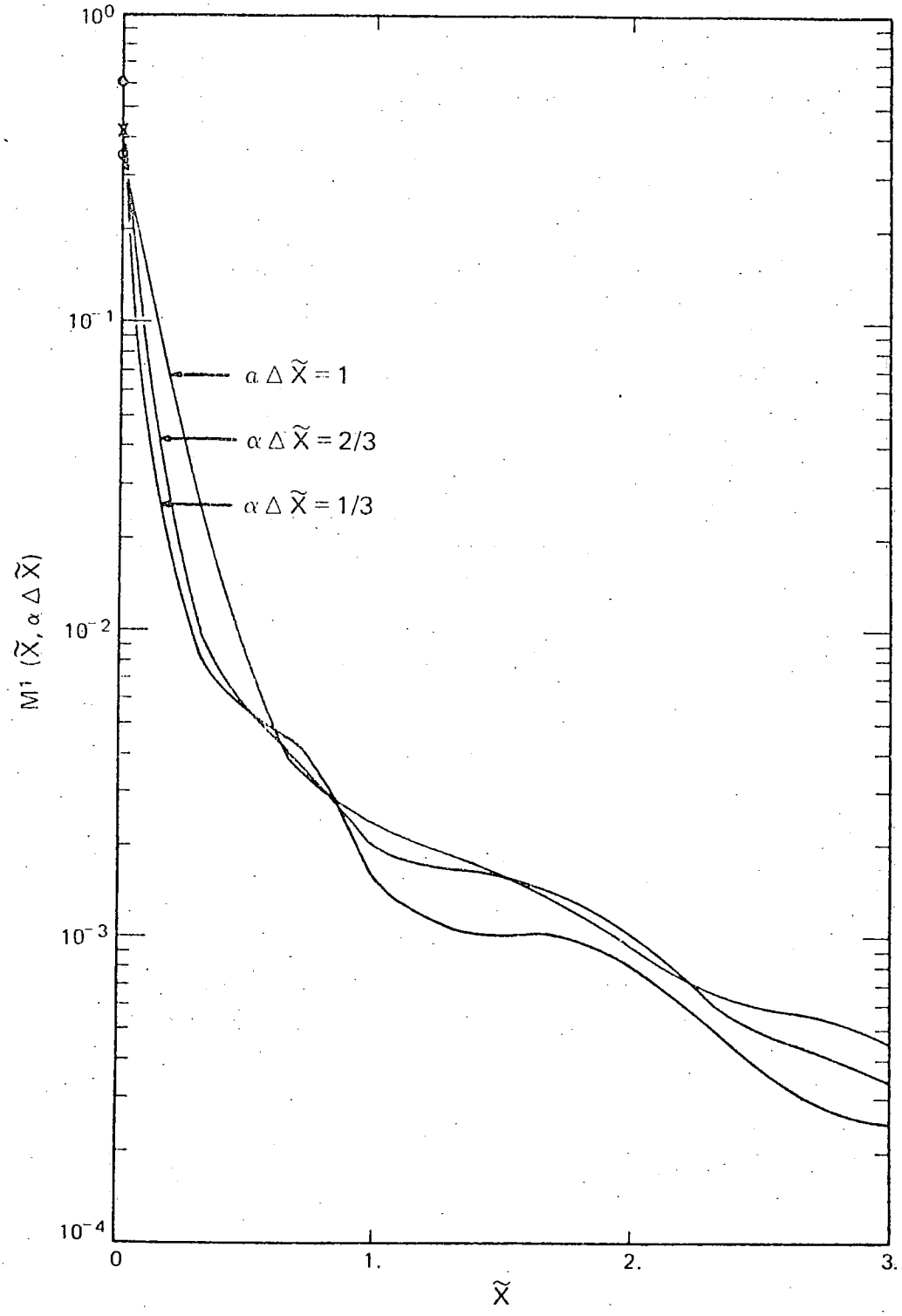

Figure 7. Prediction function for several prediction distances.

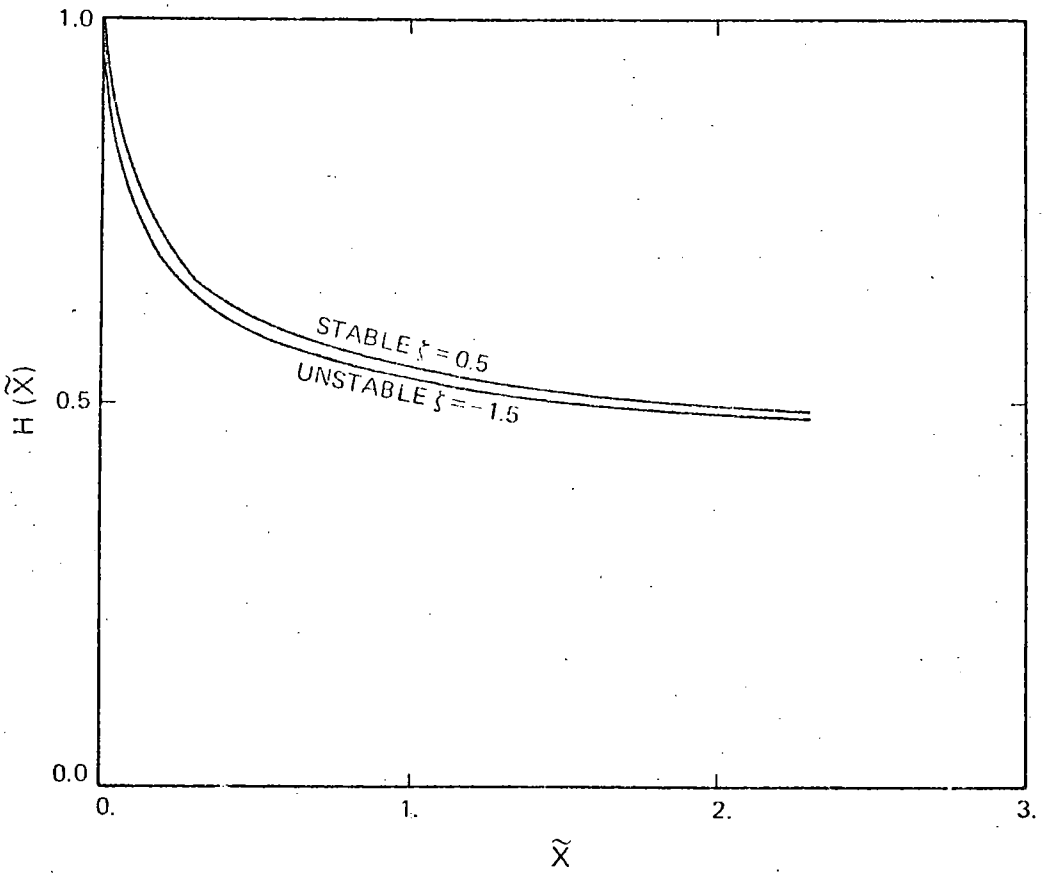

Figure 9. Correction to analytical approximation of response function to model spectrum.

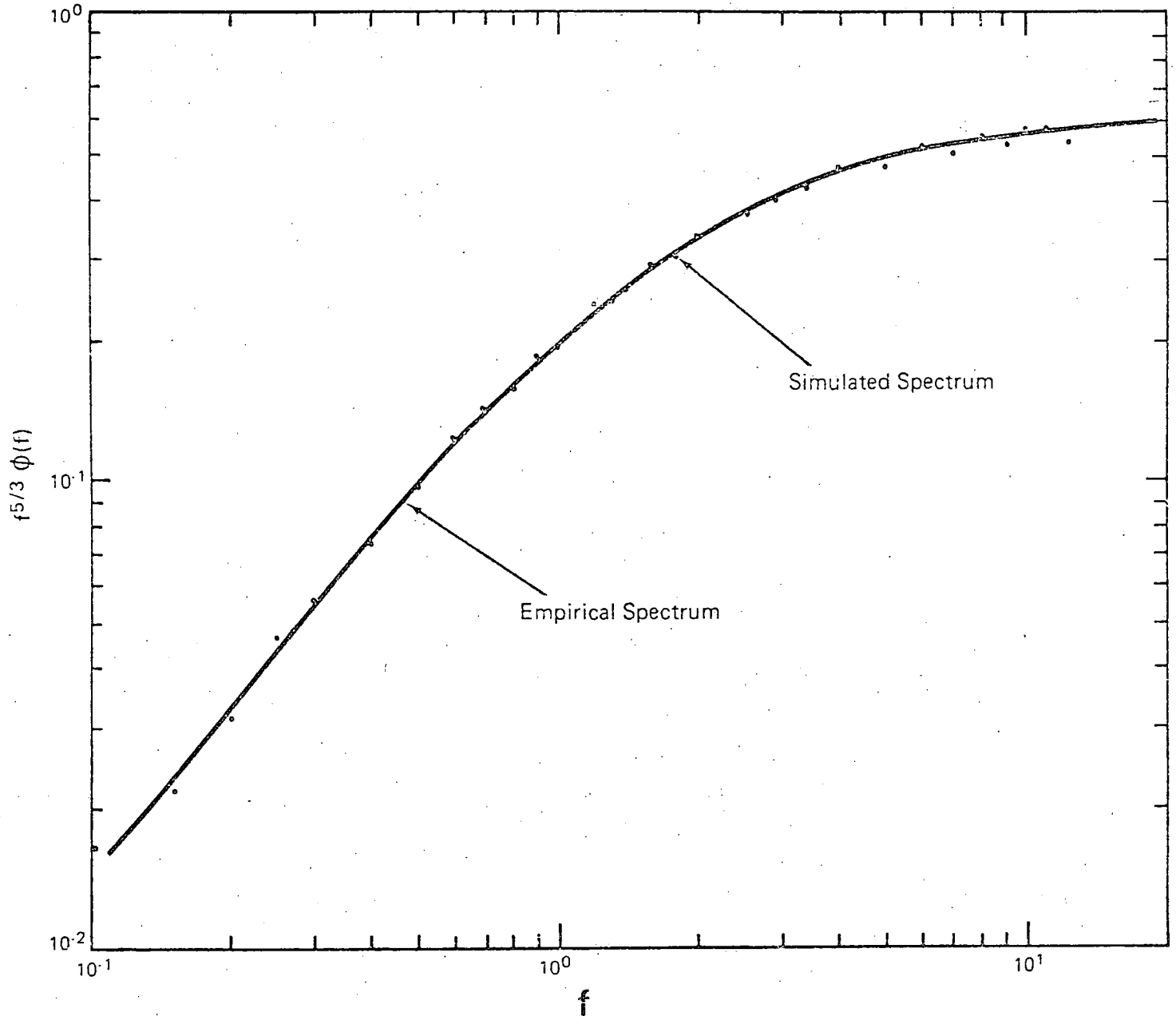

Figure 10. Comparison of w-component spectra for empirically specified model and simulated turbulence.

Acknowledgments

The author would like to express his profound gratitude to all his thesis advisors at the Pennsylvania State University, and in particular to Dr. John A. Dutton, Dr. H.A. Panofsky and Dr. H. Tennekes, for their guidance and encouragement during the course of their research.